

## Optical feedback mechanisms in laser induced growth of carbon nanotube forests

M. C. D. Bock,<sup>1</sup> R. Denk,<sup>1</sup> C. T. Wirth,<sup>2</sup> P. Goldberg-Oppenheimer,<sup>2</sup> S. Hofmann,<sup>2</sup> and J. J. Baumberg<sup>1,a)</sup>

<sup>1</sup>NanoPhotonics Centre, Cavendish Laboratory, University of Cambridge, Cambridge CB3 0HE, United Kingdom

<sup>2</sup>Department of Engineering, University of Cambridge, Cambridge CB3 0FA, United Kingdom

(Received 11 July 2011; accepted 25 November 2011; published online 6 January 2012)

We study optical feedback mechanisms occurring during growth of multi-walled carbon nanotube forests on transparent substrates. Growth is realised via laser-induced chemical vapour deposition using iron nanoparticle catalysts. *In situ* Raman and reflection spectroscopy employed clearly distinguish three growth phases. In the initial seed phase, growth of carbon nanostructures increases the laser absorption and this feedback enables growth of radially orientated carbon nanotubes. Understanding the laser interaction with the growing nanostructure holds the key towards controlled growth and opens up new routes to nanostructure and nanodevice design and fabrication. © 2012 American Institute of Physics. [doi:10.1063/1.3670328]

Carbon nanotubes (CNTs) have many potential applications due to their unique properties, but these are still somewhat limited by the lack of controlled growth and integration.<sup>1</sup> The most promising and versatile CNT growth technique is catalytic chemical vapour deposition (CVD), in which transition metal nanoparticles are exposed to a gaseous carbon precursor at elevated temperatures. Global heat exposure thereby limits CNT integration pathways, in particular for complex on-chip devices with a CMOS backbone<sup>2</sup> or involving temperature sensitive flexible substrates.<sup>4</sup> A range of local heating strategies has been reported, including electrically heated cantilevers<sup>5</sup> and laser-induced chemical vapour deposition (LICVD).<sup>4–10</sup> LICVD is viable for multi- and single-walled CNTs (Ref. 11) ( $<1 \text{ mW}/\mu\text{m}^2$ ) and has been explored using lasers from the far-IR to UV (Refs. 11–13) at continuous and pulsed exposure.<sup>6</sup> The advantage LICVD has over conventional CVD is to be able to instantly modify and control the growth rate. However LICVD has been typically limited to providing heat via specific opaque substrate layers. The idea of exciting individual metallic catalyst nanoparticles via surface plasmons has been reported;<sup>7,10,11</sup> however, no convincing CNT growth result has been achieved. A key point that has been neglected in previous literature is the interaction of the depositing carbon and growing nanostructure with the laser.

Here we show that this feedback is essential to LICVD and understanding the laser interaction with the growing nanostructure holds the key towards controlled growth. We use transparent substrates at room temperature, which allows *in situ* monitoring of CNT growth through simultaneous optical and Raman spectroscopy. We focus here on Fe catalysts evaporated (1 nm) on 20 nm  $\text{Al}_2\text{O}_3$ -covered fused silica. The samples were transferred in air to a custom-built micro-optical system, consisting of a vacuum chamber (base pressure  $10^{-5}$  mbar) with leak-valve controlled gas ports and optical viewports (Fig. 1(a)). Continuous laser light ( $\lambda = 532 \text{ nm}$ ) is

focused down to a  $1 \mu\text{m}$  (measured) spot size by a  $\times 50$  long working distance objective. Reflected and scattered optical spectra are recorded from a  $2.5 \mu\text{m}$  collection spot. Absorption spectra are recorded by light transmitted from backside illumination. The sample is scanned on an *xy* positioning stage and is monitored via a CCD camera with white light illumination (Fig. 1(d)). LICVD is carried out using acetylene at pressures ranging from 0.1–2 mbar and laser powers between 10 to 180 mW ( $\pm 0.1 \text{ mW}$ ). *In situ* spectra are recorded every 2 s using white light illumination and Raman spectroscopy (at 10 mW laser power) at positions indicated in Fig. 2(a). After growth, the samples were analysed by scanning and transmission electron microscopy (SEM/TEM).

Typical growth results (Figs. 1(b)–1(d)) show CNT forests growing in concentric ring zones and radially aligned towards the centre. Growth of these structures is a

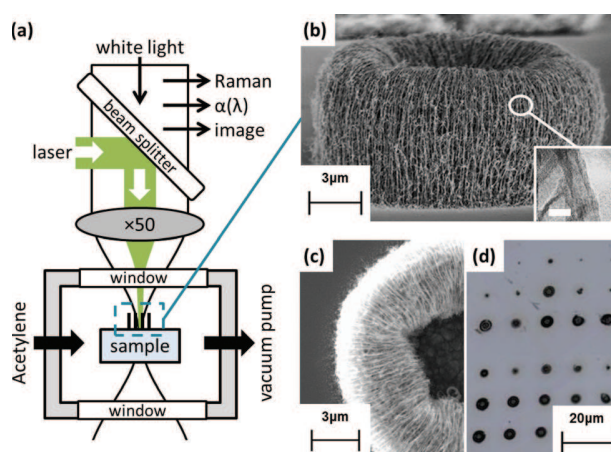


FIG. 1. (Color online) (a) Experimental setup. (b), (c) LICVD at 2 mbar acetylene using 70 mW laser power for 120 s. (b) SEM image from side ( $75^\circ$  tilted). Inset shows cross-sectional TEM image of as-grown CNTs (5 nm scale bar). (c) Top view of SEM of structure in (b). (d) Optical image with grid of optically grown nanostructures varying time and laser power.

<sup>a)</sup>Electronic mail: jjb12@cam.ac.uk.

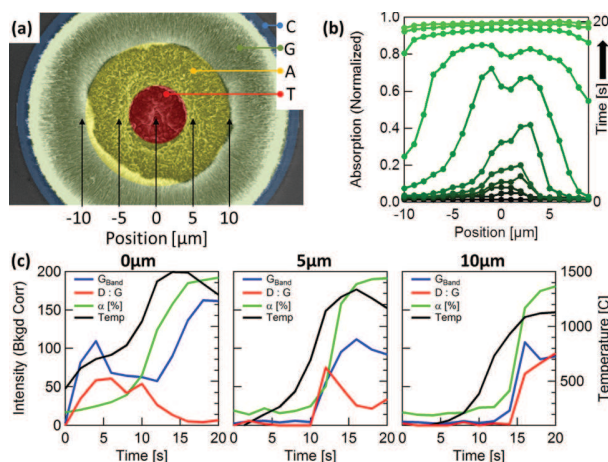


FIG. 2. (Color online) Optical growth at 0.5 mbar acetylene using 100 mW laser power for 20 s. (a) SEM with zones coloured: catalyst restructuring (C), CNT growth (G), amorphous carbon deposition (A), and graphitisation (T). (b) Absorption spectra during optical growth. (c) *In situ* tracking at different spots (0, 5, and 10  $\mu\text{m}$ ) of G band (blue), D:G % ratio (red), absorption (green), and estimated temperature (black).

consequence of strong positive optical feedback as we show below. Raman spectra (Fig. 2(c)) and SEM images (Fig. 3(a)) both independently show the presence of three separate growth phases: (i) CNT growth, (ii) amorphous carbon deposition on grown CNTs, and (iii) graphitisation of the carbon nanostructures (indicated as zones G, A, and T in Fig. 2(a)). These formations increase in diameter beyond 100  $\mu\text{m}$  with power and time. A threshold power of 70 mW is required to induce any kind of growth. Neither optical feedback growth of CNTs nor CNT forest LICVD growth in the absence of a thick thermal layer has been demonstrated previously.

Optical spectroscopy allows us to clearly distinguish different growth phases by tracking the CNT Raman bands: (i) shows an exponential increase in the G band and D:G ratio (a measure of defects in such material), (ii) a temporary steady-state marked by a sudden drop in the band growth rate, and (iii) a linear increase of G and 2D band as the D band goes to zero. It was not possible to clearly distinguish iron oxide peaks in the Raman which would provide a measure of catalyst restructuring prior to carbon deposition as seen in the SEM (region C in Fig. 2(a)). The Raman spectra at the end of 20 s are saturated in the centre (0  $\mu\text{m}$ ) and have completed their exponential rise at 10  $\mu\text{m}$  (Fig. 2(c)). During growth at high powers ( $\geq 70$  mW) the Raman signal in the centre is saturated by black body radiation ( $>700^\circ\text{C}$ ) which provides a first estimate of laser induced temperatures at the pump spot.

SEM images of a fixed sample position for increasing exposure times (Fig. 3(a)) allow analysis of the growth process result in more detail. The CNT forests emerge in the areas where newly formed CNTs are seen at earlier times and a corresponding signature is seen in the Raman and absorption spectra (Figs. 2(b) and 2(c)). Measuring the dimensions of the nanostructures in the SEM, we estimate the CNT growth rate increasing from 0.1  $\mu\text{m}/\text{s}$  to 1.1  $\mu\text{m}/\text{s}$  as optimum growth temperatures ( $750^\circ\text{C}$ ) are reached and as expected from thermally activated growth.<sup>3</sup> In regions where previously well-developed CNT forests were present we see

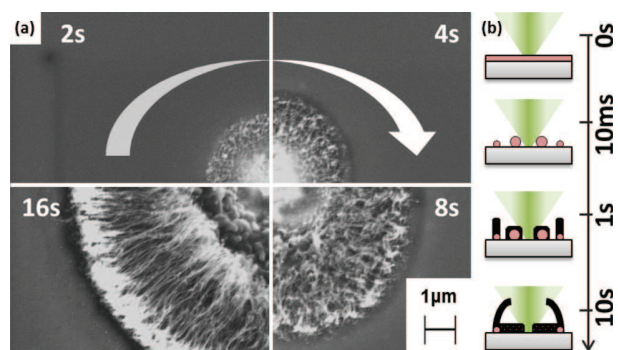


FIG. 3. (Color online) Optical growth at 0.5 mbar acetylene, 100 mW laser power. (a) Sequence of SEM images of structures viewed from top created at increasing time intervals (clockwise: 2, 4, 8, and 16 s). (b) Schematic changing morphology of sample surface during growth: initial substrate (0 s), catalyst reformation (10 ms), seed phase (1 s), and rapid growth phase (10 s). Green cone represents laser profile, iron nanoparticle catalyst (red), substrate (grey), and deposited carbon (black).

more compact arrays of carbon nanostructures. At the edge of these CNT “bulls-eyes,” the CNTs are *radially aligned* towards the centre (Fig. 1(b)). TEM of cross-sectional samples of these structures (prepared with focused ion beam) confirm that the CNTs throughout the structure are multi-walled with an average diameter of 5 nm (inset of Fig. 1(b)) and that graphitic carbon coats the CNTs in the central region.

These images match the spatial absorption profiles (Fig. 2(b)) taken at corresponding exposure times. Prior to growth the initial absorption is  $<0.1\%$ , increasing to  $>98\%$  at the end of the growth cycle as transmission drops to zero and reflectivity falls below 2%. The rate of increasing absorption becomes steeper as the boundaries move radially outwards indicating that less time is needed to reach the required CNT growth temperatures. The absorption profiles show a characteristic double peak structure, matching in size and position the torus shaped CNT structures seen in SEM (Fig. 2(a)). Both the radii of the graphitisation zone ( $r_o$ ) and CNT growth zone ( $r_o \approx 3r_i$ ) increase with time making the CNT forest rings wider with distance from the centre. Based on the measured absorption and applied laser power, we estimate the temperature profile by calculating the heat transfer for a hemispherical shell (Fig. 2(c), black lines). Heat losses due to electron emission or radiation are negligible in comparison to the surface thermal conductivity via the growing carbon structures. This model does not account for additional heating effects arising from CNTs directly absorbing laser light that induce deposition of amorphous carbon onto the CNT surfaces. LICVD of CNT forests and graphitisation is also possible on different substrates such as quartz or sapphire and in absence of any additional oxide layers. Thus, these features are reproducible and are characteristic of growth using LICVD.

To interpret these findings we discuss transformations in the catalyst layer through the LICVD process, which differs to conventional CVD growth. Initially the 1 nm Fe nanocatalyst layer is completely oxidised, with a lower absorption and reflectivity than reduced iron nanoparticles. Effective CNT growth requires Fe reduction.<sup>14</sup> Here the necessary

reducing step (since neither hydrogen nor ambient  $\sim 1$  bar acetylene pressures are present as reducing agents reported by other groups for low power LICVD (Refs. 11, 15 and 16)) is provided by the combination of high ( $\geq 70$  mW) laser powers and  $\geq 0.5$  mbar of acetylene, as confirmed by the absorption spectra (Fig. 2(b)). The iron oxide film is reduced and de-wets into islands of different diameters depending on temperature, gas type and partial pressure.<sup>17</sup>

Acetylene catalytically dissociates on the reduced and laser-heated iron. The as-formed carbon diffuses and incorporates into a graphitic lattice forming the edge of an outgrowing nanotube.<sup>14</sup> Amorphous carbon formation is a consequence of pyrolytic (in overheated zones) rather than catalytic acetylene dissociation. Positive feedback is provided since the growth of carbon structures *increases* the laser absorption, leading to rising temperatures in the local area and an exponential increase in G band (Fig. 2(c)). As the local temperature increases further ( $> 900^\circ\text{C}$ ) CNT growth is disrupted and amorphous carbon deposits on the carbon network.<sup>18</sup> The amorphous carbon coated carbon structures eventually transform into a crystalline layer as observed in SEMs which heats the newly forming CNTs on the rim, shifting the optimal zone for CNT growth radially outwards. Our understanding of the changing overall morphology *vs* time is sketched in Fig. 3(b). Fine-tuning of this process enables optical CNT forest growth within the periphery of the laser spot without the subsequent overheating sequence and graphitisation.

The annular morphology of the radially aligned CNTs (Figs. 1(b) and 3(a)) is consistent and has not been shown before. The laser focus injects heat into the catalyst nanoparticles via direct absorption in the central graphitic layer. This produces a radial temperature profile allowing more favourable conditions for CNT growth at a critical annulus. However to explain the observed radially directed growth an additional mechanism is required which induces preferential growth of CNTs oriented towards the laser focus. A second route for heating the nanoparticle catalyst anchored to the substrate is via *direct absorption* of scattered laser light by the CNTs growing out of them, acting as a “thermal antenna.” We note that CNTs growing into the laser cone are observed to thicken tenfold; hence, preferential selection of CNTs which are oriented towards the laser focus would indeed account for the radial alignment.

In this letter we demonstrate the optical mechanisms in growth of multi-walled CNT forests on transparent substrates via the use of LICVD. The increasing absorption coefficient

throughout the growth process, from reduction of the Fe catalyst to nucleation of the carbon nanostructures, constitutes strong positive feedback. This optical feedback allows us to optically detect these growth phases. Initial slow accretion is followed by a rapidly accelerating CNT growth phase producing a radially aligned CNT forest, with the CNTs growing towards the centre of the laser spot, and a subsequent graphitisation of inner carbon nanostructure as the temperature exceeds  $900^\circ\text{C}$ . Our findings provide insights to the growth mechanism of direct optical growth through *in situ* spectroscopy and are a step towards fully optically controlled growth of CNTs.

This work is supported by the UK EPSRC EP/G060649/1. R. Denk acknowledges the financial support of the Austrian Science Fund (FWF) via an Erwin Schrödinger Fellowship (J 2923-N20).

<sup>1</sup>M. S. Dresselhaus, G. Dresselhaus, P. Avouris, *Carbon Nanotubes* (Springer, Berlin, Germany, 2001).

<sup>2</sup>P. Sharma and P. Ahuja, *Mater. Res. Bull.* **43**, 2517 (2008).

<sup>3</sup>G. Zhong, S. Hofmann, F. Yan, H. Telg, J. H. Warner, D. Eder, C. Thomsen, W. I. Milne, and J. Robertson, *J. Phys. Chem. C* **113**(40), 17321 (2009).

<sup>4</sup>L. Zhu, Y. Sun, D. W. Hess, and C.-P. Wong, *Nano Lett.* **6**, 243 (2006).

<sup>5</sup>J. Lee, A. Liao, E. Pop, and W. P. King, *Nano Lett.* **9**, 1356 (2009).

<sup>6</sup>Z. Liu, D. J. Styers-Barnett, A. A. Puzos, C. M. Rouleau, D. Yuan, I. N. Ivanov, K. Xiao, J. Liu, and D. B. Geohegan, *Appl. Phys. A* **93**, 987 (2008).

<sup>7</sup>W. H. Hung, I.-K. Hsu, A. Bushmaker, R. Kumar, J. Theiss, and S. B. Cronin, *Nano Lett.* **8**, 3278 (2008).

<sup>8</sup>Y. Fujiwara, K. Maehashi, Y. Ohno, K. Inoue, and K. Matsumoto, *Jpn. J. Appl. Phys.* **44**, 1581 (2005).

<sup>9</sup>F. Rohmund, R.-E. Morjan, G. Ledoux, F. Huisken, and R. Alexandrescu, *J. Vacuum Sci. Technol. B* **20**, 802 (2002).

<sup>10</sup>D. A. Boyd, L. Greengard, M. Brongersma, M. Y. El-Naggar, and D. G. Goodwin, *Nano Lett.* **6**, 2592 (2006).

<sup>11</sup>L. Cao, D. N. Barsic, A. R. Guichard, and M. L. Brongersma, *Nano Lett.* **7**, 3523 (2007).

<sup>12</sup>I. Morjan, I. Soare, R. Alexandrescu, L. Gavrilă-Florescu, R.-E. Morjan, G. Prodan, C. Fleaca, I. Sandu, I. Voicu, F. Dumitrache, and E. Popovici, *Infrared Phys. Technol.* **51**, 186 (2008).

<sup>13</sup>K. Zimmer, R. Böhme, and B. Rauschenbach, *Physica E* **40**, 2223 (2008).

<sup>14</sup>S. Hofmann, R. Blume, C. T. Wirth, M. Cantoro, R. Sharma, C. Ducati, M. Hävecker, S. Zafeiratos, P. Schnoerch, A. Oestereich *et al.*, *J. Phys. Chem. C* **113**, 1648 (2009).

<sup>15</sup>J. B. Park, S. H. Jeong, and M. S. Jeong, *Appl. Surf. Sci.* **257**, 641 (2010).

<sup>16</sup>J. B. Park, S. H. Jeong, M. S. Jeong, S. C. Lim, I. H. Lee, and Y. H. Lee, *Nanotechnol.* **20**, 185604 (2009).

<sup>17</sup>S. Pisana, M. Cantoro, A. Parvez, S. Hofmann, A. C. Ferrari, and J. Robertson, *Physica E* **37**, 1 (2007).

<sup>18</sup>M. Picher, E. Anglaret, R. Arenal, and V. Jourdain, *Nano Lett.* **9**, 542 (2009).